NhaA antiporter functions using 10 helices, and an additional 2 contribute to assembly/stability

Etana Padan[a,1], Tsafi Danieli[b], Yael Keren[b], Dudu Alkoby[a], Gal Masrati[c], Turkan Haliloglu[d], Nir Ben-Tal[c], and Abraham Rimon[a]

[a]Department of Biological Chemistry, Alexander Silberman Institute of Life Sciences, Hebrew University, 91904 Jerusalem, Israel; [b]Protein Expression Facility, Wolfson Centre for Applied Structural Biology, Alexander Silberman Institute of Life Sciences, Hebrew University, 91904 Jerusalem, Israel; [c]Department of Biochemistry and Molecular Biology, George S. Wise Faculty of Life Sciences, Tel-Aviv University, Ramat Aviv 69978, Israel; and [d]Department of Chemical Engineering, Polymer Research Center, Bebek 34342, Boğaziçi University, Istanbul, Turkey

Edited by H. Ronald Kaback, University of California, Los Angeles, CA, and approved August 27, 2015 (received for review June 17, 2015)

The *Escherichia coli* Na^+/H^+ antiporter (Ec-NhaA) is the best-characterized of all pH-regulated Na^+/H^+ exchangers that control cellular Na^+ and H^+ homeostasis. Ec-NhaA has 12 helices, 2 of which (VI and VII) are absent from other antiporters that share the Ec-NhaA structural fold. This α-hairpin is located in the dimer interface of the Ec-NhaA homodimer together with a β-sheet. Here we examine computationally and experimentally the role of the α-hairpin in the stability, dimerization, transport, and pH regulation of Ec-NhaA. Evolutionary analysis (ConSurf) indicates that the VI–VII helical hairpin is much less conserved than the remaining transmembrane region. Moreover, normal mode analysis also shows that intact NhaA and a variant, deleted of the α-hairpin, share similar dynamics, suggesting that the structure may be dispensable. Thus, two truncated Ec-NhaA mutants were constructed, one deleted of the α-hairpin and another also lacking the β-sheet. The mutants were studied at physiological pH in the membrane and in detergent micelles. The findings demonstrate that the truncated mutants retain significant activity and regulatory properties but are defective in the assembly/stability of the Ec-NhaA dimer.

transport protein | helices truncation | Na^+/H^+ antiporter/NhaA | elastic network model | ConSurf

Living cells are critically dependent on processes that regulate intracellular pH, Na^+, and volume (1), and Na^+/H^+ antiporters play a primary role in these homeostatic mechanisms (reviewed in ref. 2). These antiporters are found in the cytoplasmic and intracellular membranes of most organisms (reviewed in refs. 3–6), and they have long been human drug targets (7).

The principal Na^+/H^+ antiporter in *Escherichia coli*, Ec-NhaA, is responsible for intracellular Na^+ and H^+ homeostasis (8), and homologs have recently been implicated in the virulence of pathogenic bacteria (9). In humans, orthologs have been suggested to be involved in essential hypertension (10), as well as diabetes (11).

Ec-NhaA is characterized by exceptionally high transport activity (12), a stoichiometry of $2H^+/Na^+$ (13), and strong pH dependence (12), a property shared with other prokaryotic (8) and eukaryotic Na^+/H^+ antiporters (reviewed in refs. 3–6). Crystal structures of down-regulated Ec-NhaA at acidic pH (14) (Fig. 1) reveal a unique structural fold shared by a growing number of secondary transporters (15, 16, 17).

Omitting transmembrane segments (TMs) VI and VII, the remaining 10 TMs of monomeric Ec-NhaA are organized into a highly conserved, densely packed core domain composed of two structurally related helix bundles (TMs III, IV, and V and TMs X, XI, and XII) that are topologically inverted with respect to each other (Fig. 1*B*) (14). TMs IV and XI are each interrupted by an unwound chain that crosses the other chain in the middle of the membrane, leaving two short helices oriented toward the cytoplasm (c) or the periplasm (p) (IVc, IVp and XIc, XIp, respectively; Fig. 1) (14). This noncanonical TM assembly—the NhaA fold—creates a delicately balanced electrostatic environment in the middle of the membrane at the ion binding site(s), which likely plays a critical role in cation exchange activity. The other TMs—the dimer interface domain—comprise a bundle along the dimer interface and also contain inverted-topology repeats (TMs I, II and VIII, IX; Fig. 1*B*) (18).

Interestingly, the Na^+/H^+ antiporter structures that share the NhaA fold are characterized by different numbers of TMs from 12 to 13 (16, 17, 19) and are dimeric like Ec-NhaA. However, two prokaryotic ASBT (apical sodium-dependent bile acid transporter, also known as SLC10A2) symporters share the NhaA fold but have only 10 TMs; they lack the Ec-NhaA equivalents of helices VI and VII (20, 21). The ASBTs also differ from Ec-NhaA in that they are Na^+/bile acid symporters. In addition, the ASBTs are monomeric. Taken together, the data raise questions regarding the role of TMs VI and VII in Ec-NhaA.

In Ec-NhaA, helices VI and VII, which form an α-hairpin, are located in the dimer interface (Fig. 1 *B* and *C*). Therefore, these substructures may contribute to NhaA dimerization and/or stability; however, data in this regard are not available. In the current study, we constructed an NhaA mutant deleted of TMs VI and VII and studied its properties at physiological pH. The mutant devoid of TMs VI and VII is defective with respect to dimerization and/or stability but exhibits decreased but significant transport activity, as well as pH regulation.

Results

The TM VI–VII Hairpin Is Not Conserved. Evolutionary conservation is often indicative of importance for structure and/or function. Therefore, to obtain preliminary insight regarding the potential importance of TMs VI and VII, ConSurf (22) (consurf.tau.ac.il) was used to estimate evolutionary conservation of these helices

Significance

The principal Na^+/H^+ antiporter of *Escherichia coli* (Ec-NhaA) is the best-characterized of the pH-regulated Na^+/H^+ exchangers that control cellular Na^+ and H^+ homeostasis, and the human homologues are potentially important drug targets. Identification of the essential components of NhaA is vital to understanding the function of the protein and has implications for evolution and protein design. Ec-NhaA has 12 helices, 2 of which (VI and VII) are absent from the growing number of secondary transporters that share the unique Ec-NhaA structural fold. Mutants deleted of helices VI and VII, which form an α-hairpin at the dimer interface, are defective in the assembly/stability of the Ec-NhaA dimer but retain significant transport activity, as well as regulatory properties.

Author contributions: E.P., T.H., and N.B.-T. designed research; E.P., T.D., Y.K., D.A., G.M., T.H., and A.R. performed research; T.D. contributed new reagents/analytic tools; E.P., T.H., and N.B.-T. analyzed data; and E.P. and N.B.-T. wrote the paper.

The authors declare no conflict of interest.

This article is a PNAS Direct Submission.

[1]To whom correspondence should be addressed. Email: etana@vms.huji.ac.il.

This article contains supporting information online at www.pnas.org/lookup/suppl/doi:10.1073/pnas.1510964112/-/DCSupplemental.

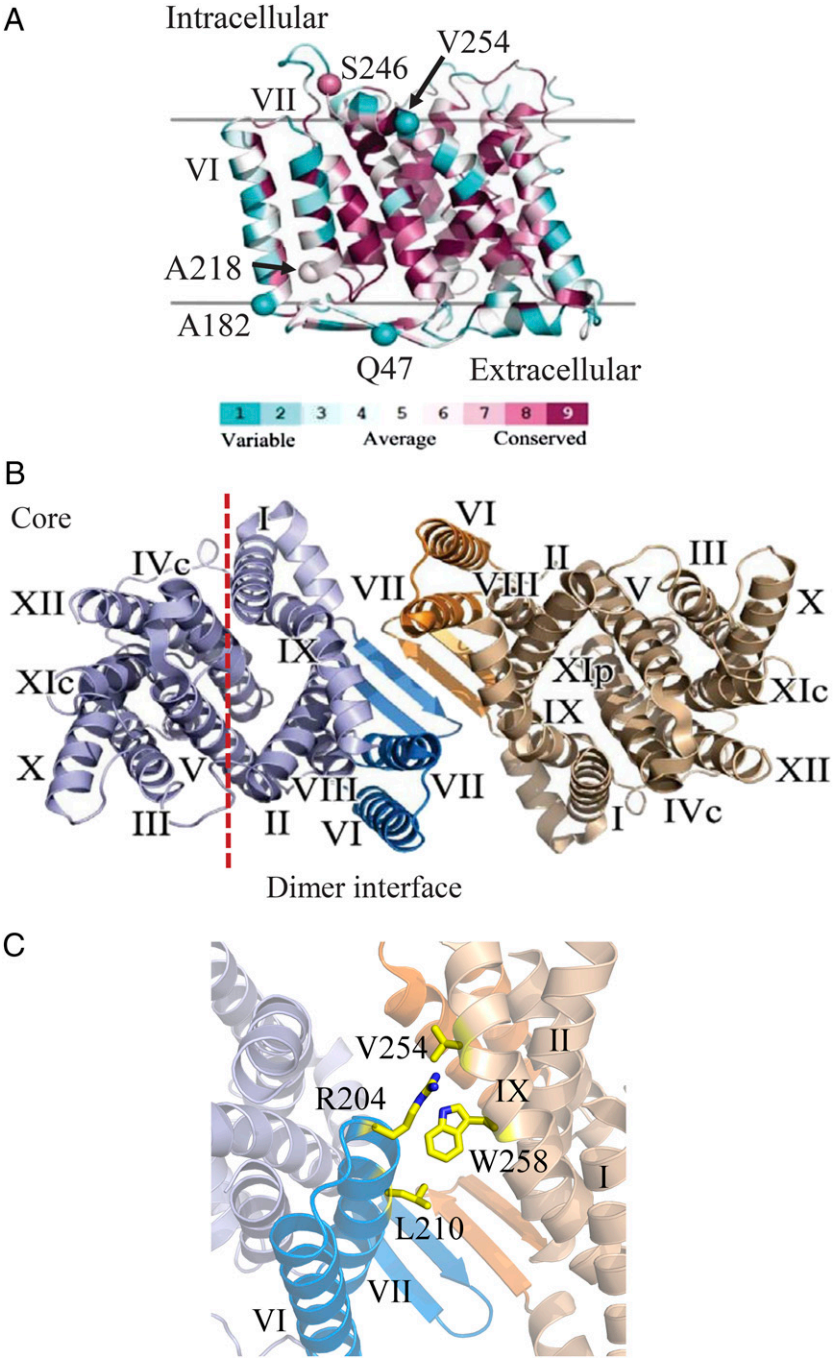

Fig. 1. (*A*) Evolutionary conservation analysis of Ec-NhaA. The crystal structure of Ec-NhaA, in ribbon representation, as seen in the plane of the membrane, represented with gray outlines, with the intracellular side facing up. ConSurf analysis (consurf.tau.ac.il) was carried out using PDB ID code 1ZCD (14). The amino acids are colored by their conservation grades using the color-coding bar, with cyan through maroon indicating variable through conserved. Overall, helices VI and VII, denoted with roman numerals, are of the least conserved TM helices with average conservation scores of 1 and 5, respectively, according to the ConSurf scoring method. The sites of the three single amino acid mutations Q47C, S246C, and V254C and the two sites in which Ec-NhaA was truncated (A182 on and A218 on) are shown as spheres (*B*) Ec-NhaA dimer. The crystal structure of the Ec-NhaA dimer (27), PDB ID code 4AU5, in ribbon representation as seen from the cytoplasm, with TM helices numbered as in *A*. The first monomer is colored light blue and the second colored wheat. The α-hairpin (composed of helices VI and VII) and β-sheet of one monomer are highlighted in marine and in the other monomer in orange. The red dashed line marks the boundary between the two functional domains of the transporter, the core domain to the left and the panel/dimer interface to the right. As can be seen the α- and β-hairpins constitute the dimer interface. (*C*) Close-up view on the interaction between the monomers. The Ec-NhaA dimer interface is shown as ribbon representation, with monomers colored as in *B*. Although the β-hairpin contributes the majority of interactions between subunits from the extracellular side, there is also a small interface between the cytoplasmic ends of helix VII of one monomer and helix IX of the other. This interaction probably involves hydrogen bond and hydrophobic contacts and forms a zipper-like structure consisting of R204 and L210 of one monomer and V254 and W258 of the other (27). The figures were generated using PyMol (PyMOL Molecular Graphics System, version 1.7.4; Schrödinger, LLC) (47, 48).

(Fig. 1). TMs VI and VII are among the least conserved TMs of Ec-NhaA (Table S1), suggesting that these helices may be dispensable.

Normal Mode Analysis. Normal mode analysis (NMA) was applied to analyze the dynamics of the Ec-NhaA protein computationally by using the Gaussian network model (GNM) (23). In GNM the protein structure is approximated as a connectivity matrix in which nodes correspond to the Cα atoms, and springs connect Cα atoms that are located at a specific distance from each other. The particular architecture of the protein is the sole factor determining the collective modes of motion. The calculations were conducted using the commonly used distance cutoff of 10 Å between the Cα atoms of the side chains. We analyzed the two NhaA structures (PDB ID codes 1zcd and 4au5), and very similar results were obtained whether monomers or homodimers were used as models. We present only results obtained using the PDB ID code 1zcd. A previous study (18) using NMA to study Ec-NhaA suggested that the two slowest modes of motion are associated with pH-induced conformational changes. Here the results obtained with native Ec-NhaA and structurally related Nm-ASBT (20) are compared with NMA of a virtual mutant of Ec-NhaA in which TMs VI and VII (Ala182 to Ala208, Fig. 1*A*) were deleted.

Truncated Ec-NhaA, native Ec-NhaA, and ASBT show dynamic modes with very similar eigenmode spectra (Fig. S1). In particular, the two slowest modes are outstandingly high in the spectra (mode indices 1 and 2) and are generally similar for the three proteins (Fig. S2 and Table S2). The slowest mode identified for each protein separates the antiporter into two dynamic domains, connected by a hinge (Fig. S3 *A*–*C*). In ASBT and native Ec-NhaA, the dynamic domains overlap with the dimer interface domain and the core structural domain. The hinge is narrow and aligns with the anticipated membrane normal (Fig. S3 *B* and *C*). In truncated Ec-NhaA the hinge region is much broader and tilted (Fig. S3*A*). In native Ec-NhaA the hinge includes amino acids 164–171 (TM V) and 264–270 (TM IV), which are known to be involved in Ec-NhaA function (24). Of these, amino acids 168–171 persist as hinges upon truncation of the helical hairpin (Fig. S3*A*). Because dynamics are essential for activity, it is tempting to suggest that truncated Ec-NhaA may retain significant antiport activity.

In each of the transporters, the second-slowest mode, similarly to the first-slowest mode, also separates the structure into two dynamic domains (Fig. S3 *D*–*F*). In ASBT the hinge plane is roughly along the membrane midplane (Fig. S3*F*), and in native and truncated Ec-NhaA it is diagonal (Fig. S3 *D* and *E*). In native Ec-NhaA the hinge includes amino acids 135–136, 261, and 336, known to be involved in ion translocation (24). This is an indication of the importance of the second-slowest mode for translocation. The composition of the hinge in truncated Ec-NhaA differs from that in native Ec-NhaA; specifically, it comprises a different set of amino acids, which are also implicated in ion translocation: 150–156, 166–167, and 264–266 (24).

Ec-NhaA forms homodimers (reviewed in ref. 2), and truncation may have an effect on dimerization. The dimer is held together by interactions between the β-hairpins that form a β-sheet between the two monomers (25, 26), and the crystal structure of the dimer shows (27) that TM VII may also contribute to interactions between monomers in the dimer interface. The reduced cooperativity of monomeric Ec-NhaA upon truncation (*SI Text, Extended NMA Results*) may also have indirect effects on dimerization. In any event, the analysis suggests overall that truncated Ec-NhaA may be less stable than native Ec-NhaA.

Deletion of TM IV and VII. Based upon the evolutionary analysis and NMA, a mutant, Δ(VI-VII), was constructed in which the DNA encoding TMs VI to VII was deleted (Ala182–Ala218, Fig. 1*A*). In addition, a previously described mutant deleted of the β-sheet (Pro45–Asn58) (25) was used to construct the double mutant Δ(VI-VII/β).

To characterize the mutants phenotypically (Table 1 and Fig. 2), *E. coli* EP432 (*nhaA*$^-$ *nhaB*$^-$) (28) cells were each transformed with plasmid encoding a given Ec-NhaA mutant or were mock-transformed (as negative controls), and the cells were tested for expression in the membrane and growth on Na^+- or Li^+-selective media at neutral or alkaline pH (Fig. 2). Both mutants, Δ(VI-VII) and Δ(VI-VII/β), were expressed significantly (35.0 and 7.5%, respectively, compared with the expression level of the WT; Table 1 and Fig. 2). Because all variants were expressed from a multicopy plasmid, even the low level of expression is far above the level expressed from the single chromosomal gene that confers an Na^+-resistant phenotype (29). Clearly, cells transformed with mutant Δ(TM VI-VII) grow almost as well as the WT on normal LBK medium and at neutral pH in the presence of high concentrations of Na^+ or Li^+. However, in contrast to the WT, which grows in the presence of high concentrations of Na^+ or Li^+ at alkaline pH, mutants Δ(TM VI-VII) and Δ(TM VI-VII/β), like the mock-transformed control, do not grow under these conditions (Table 1).

Na^+/H^+ Antiport Activity in Isolated Membrane Vesicles. Na^+/H^+ and Li^+/H^+ antiport activity were measured in everted membrane vesicles isolated from *E. coli* EP432/pΔ(VI-VII) and EP432/pΔ(VI-VII/β) cells. Cells transformed with plasmid pAXH3 encoding WT Ec-NhaA or with the empty pBR322 plasmid served as positive and negative controls, respectively (Fig. 3*A* and Table 1). Antiport activity was estimated from the change in ΔpH (interior acid) elicited by addition of Na^+ or Li^+, our standard assay, which uses acridine orange fluorescence. Specifically, after generating ΔpH by oxidation of D-lactate (Fig. 3*A*, arrow pointed downward), quenching of acridine orange fluorescence is observed when Na^+ or Li^+ (Fig. 3, arrow pointed upward) was added to vesicles containing a functional Na^+/H^+ antiporter. Activity (maximal dequenching) was determined for each condition listed in Table 1. Mutant Δ(VI-VII) exhibits ∼49 and ∼36% of WT activity with either Na^+ or Li^+, respectively (Table 1). Mutant Δ(VI-VII/β) was somewhat less active, exhibiting ∼33 or ∼36% of WT activity with Na^+ or Li^+, respectively. Remarkably, apparent K_ms for Na^+ with both mutants is ∼0.1 mM NaCl, very similar to that of WT. In contrast, the apparent K_m for Li^+ with both mutants is also ∼0.1 mM LiCl, which is about five times higher than that of the WT (Table 1). Hence, deletion of TM VI and VII from Ec-NhaA has no effect on the apparent K_m for Na^+ but causes a somewhat increased K_m for Li^+.

The pH dependence of the Na^+, Li^+/H^+ antiport activity of both mutants was also measured in isolated everted membrane vesicles and is very similar to that of WT Ec-NhaA (Fig. 3*B*). Specifically, both mutants manifest very low activity below pH 6.5 and maximal activity is observed at ∼pH 8.5. Antiport activity was measured at either 10 or 100 mM NaCl or LiCl with similar results.

Na^+/H^+ Antiport Activity in Proteoliposomes. The stoichiometry of WT Ec-NhaA is $2H^+/1Na^+$; therefore, the antiport activity of EcNhaA is electrogenic (12). Like other electrogenic secondary transporters, activity is sensitive to the presence of a membrane potential (1). Therefore, when WT Ec-NhaA is reconstituted into proteoliposomes and ΔpH-driven ^{22}Na uptake is determined in the absence of a permeant ion, activity is low because of the antiport reaction itself generates a ΔΨ (interior negative) that inhibits turnover (Fig. 3*C*). However, when the membrane is made permeant to K^+ by the ionophore valinomycin, the ΔΨ is dissipated and a marked increase in both the rate and steady-state level of Na^+ transport is observed (ref. 12 and Fig. 3*C*). Surprisingly, although mutant Δ(VI-VII) in isolated membrane vesicles exhibits ∼50% of the Na^+/H^+ antiport activity of the WT antiporter with similar kinetic parameters (Table 1 and Fig. 3 *A* and *B*), the activity of the mutant in proteoliposomes is only ∼10% of the WT, and K^+ plus valinomycin increases activity approximately twofold (Fig. 3*C*).

Table 1. Expression level, growth phenotype, and Na^+/H^+ antiporter activity of Ec-NhaA truncated mutants

NhaA mutants	Expression (% of WT)	Growth 0.6 M Na^+ 0.1 M Li^+ pH:				K_m (pH 8.5), mM		Activity (% dequenching), pH 8.5	
		7	8.2	7	8.2	Na^+	Li^+	Na^+	Li^+
Δ(VI-VII)	35.0	+++	—	++	—	0.11	0.10	49	36.4
Δ(VI-VII/β)	7.5	+++	—	++	—	0.12	0.13	36	33
WT	100	+++	+++	+++	+++	0.5	0.02	100	100
Vector	0	—	—	—	—	ND	ND	—	—

For characterization of Ec-NhaA mutants, *E. coli* EP432 cells were transformed with plasmids expressing the indicated variants. The positive and negative controls were cells transformed with pAXH3 expressing WT NhaA and pBR322 (the empty vector), respectively. Expression level in the membrane is expressed as percentage of control cells (WT). Growth experiments were conducted at 37 °C on LB modified agar plates containing 0.6 M NaCl at pH 7 or pH 8.2 or 0.1 M LiCl at pH 7 or pH 8.2. +++, number and size of the colonies after 48 h of incubation of the control; ++, same number of colonies as the control but smaller in size; +, both size and number of colonies reduced compared with controls; —, no growth. The apparent K_m for the ions was determined at pH 8.5, as described in *Materials and Methods*. Na^+/H^+ and Li^+/H^+ antiporter activity in everted membrane vesicles at pH 8.5 was determined with 10 mM NaCl or LiCl. Activity is expressed as percentage of dequenching. ND, not determined.

Dimerization in the Membrane and in Detergent Micelles. WT Ec-NhaA is a stable dimer in the membrane (30, 31) and in *n*-dodecyl-β-D-maltopyranoside (DDM) micelles (25, 27), and the dimer interface has been identified by intermolecular cross-linking (26, 31). Thus, when a single amino acid in each NhaA monomer at the dimer interface is replaced with Cys (Fig. 1*A*; V254C, S246C, or Q47C), that Cys residue cross-links with its twin in the other monomer (26, 31). These Cys replacements were introduced into mutant Δ(VI-VII), and cross-linking was studied with bifunctional cross-linkers of different lengths, all of which yield similar results (Fig. 4*A*). In agreement with previous results that the β-sheet, which remains in this mutant, is primarily responsible for dimerization, mutant Δ(VI-VII)-Q47C, like mutant Q47C (26), exhibits very significant cross-linking (Fig. 4*A*), implying that the β-sheet remains intact in the mutant. Likewise, in the mutant as in the WT (31), a single Cys replacement in Δ(VI-VII)-S246C, in loop VIII–IX on the cytoplasmic side, cross-linked its twin Cys. In marked contrast, whereas in the WT a single Cys replacement in TM IX on the cytoplasmic side (WT-V254C) cross-links very efficiently, very low cross-linking was observed with Δ(VI-VII)-V254C (Fig. 4*A*).

To determine the oligomeric state of mutant Δ(TM VI-VII) in DDM, the protein was affinity-purified and subjected to native gel electrophoresis (Fig. 4*B*, *Right*). Although the mutant still possesses the β-sheet on the periplasmic side of the protein, purified mutant Δ(VI-VII) in DDM micelles is monomeric. This result indicates that TMs VI and VII of the monomers are essential for maintaining the stability of the dimer in DDM micelles.

WT Ec-NhaA protein in DDM detergent micelles denatures at temperatures above 62.5 °C (26) and, like many other membrane proteins, the protein aggregates at denaturing temperatures (Fig. 4*B*, *Left*). In marked contrast, the truncated mutant begins to aggregate at 55 °C and is essentially completely aggregated at 65 °C (Fig. 4*B*, *Middle*). Hence, in DDM micelles, the Δ(TM VI-VII) mutant is considerably less stable than the WT protein.

Despite many trypsin-cleavable sites in the primary protein sequence, WT Ec-NhaA is remarkably resistant to trypsin below pH 7 both in the membrane and in DDM micelles. Furthermore, at pH 8.5, only one trypsin-cleavable site is observed at Lys249 (32), and two fragments are observed (Fig. 4*C*, 24.0 and 16.0 kDa). In addition, the pattern of trypsin cleavage in certain

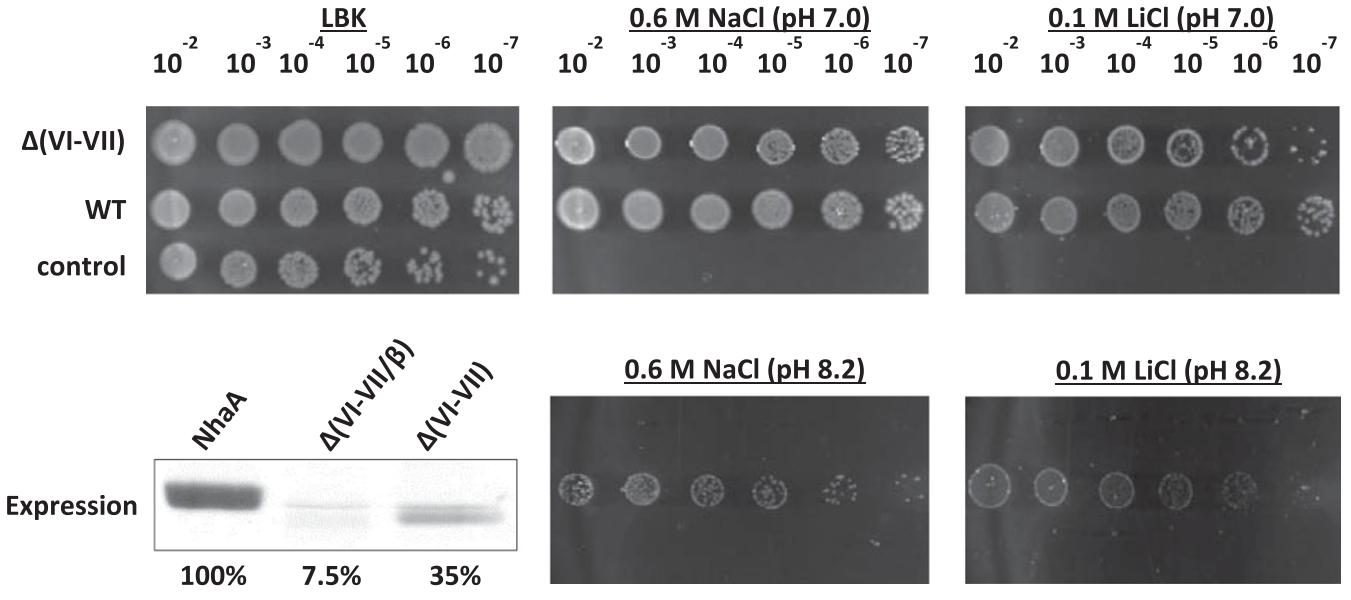

Fig. 2. Expression and growth phenotype of the truncated NhaA mutant. Growth of *E. coli* EP432 transformed with plasmids expressing the mutant Δ(VI-VII) or WT on nonselective agar plates of LBK and on selective agar media was as indicated. The control was EP432/pBR322. Expression level of the proteins in isolated membrane vesicles of the respective strains was as described in *Materials and Methods* and expressed as percent of WT (100%).

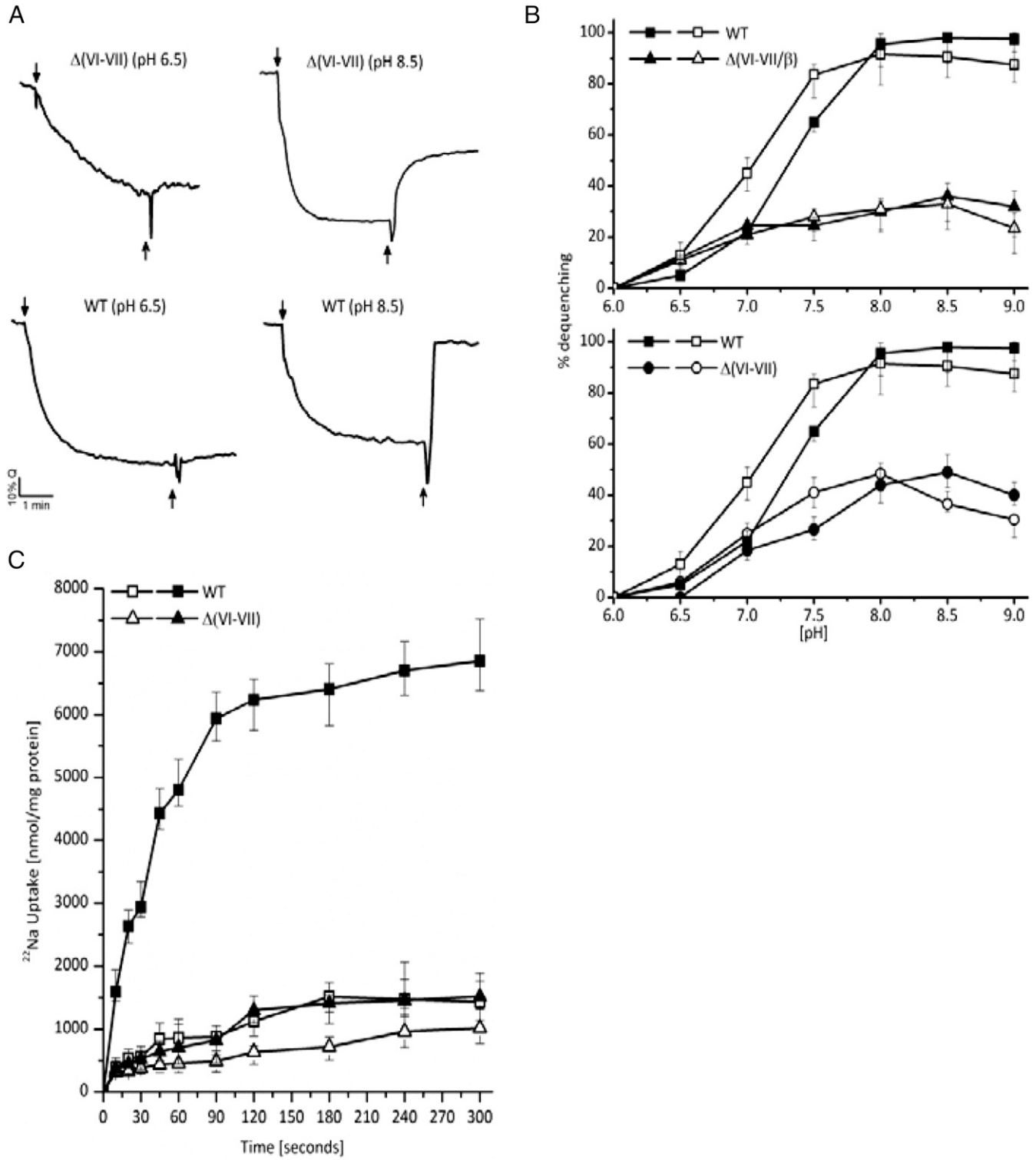

Fig. 3. The Na^+/H^+ and Li^+/H^+ antiporter activity of Δ(TM VI-VII) mutant is similar to that of the WT in the membrane but not in proteoliposomes. (*A*) Everted membrane vesicles were prepared from EP432 cells grown in LBK (pH 7) and transformed with plasmids expressing WT or Δ(VI-VII) as indicated. The Na^+/H^+ and Li^+/H^+ antiporter activity was determined in the presence of 10 mM of Na^+ or Li^+ at the indicated pH values. For example, after energization with D-lactate (2 mM), fluorescence was quenched (downward-pointing arrow) and achieved a steady state, and then 10 mM of Na^+ was added (upward pointed arrow). A reversal of the fluorescence level (dequenching) indicates that protons are exiting the vesicles in antiport with Na^+. All experiments were repeated at least three times with nearly identical results. (*B*) Everted membrane vesicles were prepared from EP432 cells transformed with mutant Δ(VI-VII/β) (*Upper*) and mutant Δ(TM VI-VII) (*Lower*) and the Na^+ (10 mM, filled symbols) and Li^+ (10 mM, empty symbols) antiport activity was measured at the indicated pH levels. All experiments were repeated at least three times with nearly identical results. The error bars (representing SD) are shown on the graphs. (*C*) The affinity-purified proteins of WT (square symbols) and Δ(VI-VII) (triangle symbols) proteins were reconstituted into proteoliposomes and ΔpH (acidic inside)-driven ^{22}Na uptake was determined as described in *Materials and Methods*. The reaction mixture (500 μL) contained 150 mM choline chloride, 10 mM Tris/Hepes (pH 8.6), 2 mM MgS04, 10 mM KCl, and 50 mM $^{22}NaCl$ (1 mCi/mL). Where indicated (filled symbols), valinomycin (5 μM) was added from zero time. The error bars representing SD are shown on the graphs.

mutants reflects differences in the pH-induced conformational change in Ec-NhaA (32, 33). In striking contrast to the WT, mutant Δ(VI-VII) is cleaved by trypsin at both neutral and alkaline pH, and as expected the heavy fragment from the deletion mutant exhibits lower apparent MWs than the WT.

Discussion

Secondary transporters with the NhaA fold have different numbers of TM helices (16, 19–21). For example, the ASBT symporter with 10 TM helices does not contain equivalents for helices VI and VII found in Ec-NhaA (20, 21), which has 12 TM helices (14). Therefore, we postulated that each transporter may have a minimal conserved core responsible for transport function and that the two additional helices in Ec-NhaA are "accessories" that provide a secondary function. To address this problem, we initiated computational studies, which indicate that deletion of TMs VI and VII from Ec-NhaA has relatively minor effects on the dynamics of the antiporter, and stronger effects on the stability/assembly of the tertiary structure (i.e., dimerization). Our computational studies support the hypothesis with the following observations. (*i*) Evolutionary conservation analysis shows that TM helices VI and VII are the least conserved TM helices in the antiporter (Fig. 1*A* and Table S1). (*ii*) NMA suggests that truncated, native Ec-NhaA and the ASBT symporter are characterized by very similar dynamics (Figs. S1–S4) and cooperativity (Figs. S4 and S5). (*iii*) Both dynamics in the dimer interface region (Figs. S3–S5) and cooperativity are altered by truncation of TM helices IV and VII (Figs. S4 and S5). The conclusions offered by these computational studies are consistent with previous crystal structure-based data and with the biochemical findings also presented here.

The Ec-NhaA crystal structure (14, 27) shows that the interface domain contacts between the two monomers at only two sites (25, 27) (Fig. 1 *B* and *C*): At the periplasmic side, the β-hairpins form a β-sheet parallel to the membrane. At the cytoplasmic side, the contacts are formed by very few residues in TM VII of one monomer and in TM IX of the other monomer. The space left at the dimer interface is probably filled with lipids (27).

We have previously shown that it is possible to delete the β-hairpin of the Ec-NhaA dimer interface domain, and the resultant mutant Δβ is monomeric and fully functional. Only under extremely stressful growth conditions does the WT Ec-NhaA dimer grow better than the monomer (25, 26). Hence, the functional unit of Ec-NhaA is monomeric and is a stable monomer in the native membrane, in proteoliposomes, and in DDM micelles and is fully functional under each condition.

Here we reveal that it is also possible to delete two helices (VI and VII) of the interface domain and yet obtain a functional antiporter in membrane vesicles. We truncated the two helices alone and in combination with the Δβ mutation and obtained the mutants Δ(VI-VII) and (Δ(TM VI-VII/β), respectively. Similarly to the Δβ mutant (25), the Δ(VI-VII) and (Δ(TM VI-VII/β) mutants are expressed at reasonable levels in the cytoplasmic membrane (Table 1 and Fig. 2) and exhibit antiport activity (Fig. 3*A*) with a pH dependence very similar to that of the WT (Table 1 and Fig. 3*B*). Remarkably, the apparent K_m for Na^+ obtained for these mutants in inverted membrane vesicles is identical to that of the WT and of the Δβ mutant (Table 1). However, our results also show that elimination of the contacts between monomers on the cytoplasmic side by deletion of helices VI and VII apparently has a much more drastic effect on Ec-NhaA compared with deletion of the β-sheet on the periplasmic side (refs. 25 and 26 and Table 1): Although mutant Δ(VI-VII) is a dimer in the membrane, in situ cross-linking data (Fig. 4*A*) show that this dimer differs from the WT dimer on the cytoplasmic side. Therefore, the truncated dimer may be less stable than the WT, and, indeed, this seems to be the case for the following reasons. (*i*) In DDM micelles under native gel electrophoresis, purified WT Ec-NhaA exhibits much slower mobility compared with the truncated mutant (Fig. 4*B*, *Right*). (*ii*) WT Ec-NhaA is trypsin-insensitive at pH 7.5 and exhibits a single unique trypsin cleavage site at pH 8.5 (ref. 32 and Fig. 4*C*). In contrast, mutant Δ(VI-VII) is cleaved by trypsin at both pHs. (*iii*) The truncated mutant aggregates at a lower temperature than the WT does (Fig. 4*B*). (*iv*) The truncated mutant has much lower antiport activity than the WT does after solubilization, purification, and reconstitution (Fig. 3*C*). Therefore, the overall picture suggests that although the truncated mutant forms a dimer in the membrane that has good activity, the dimer is unstable and dissociates more readily than the WT dimer does and therefore is less active in DDM micelles.

Taken together, our results show that contacts in the Ec-NhaA dimer on both the cytoplasmic and periplasmic sides are not important for functionality but are important for proper assembly/stability of the dimer. The contacts on the cytoplasmic side are more critical than those on the periplasmic side; it is possible that because the β-sheet is external to the protein on the periplasmic side (14, 27), its deletion has a less deleterious effect on the structure compared with deletion of helices VI and VII. Indeed, the double-mutant Δ(VI-VII/Δβ) exhibits properties that do not differ substantially from those of mutant Δ(VI-VII) (Table 1 and Fig. 3*B*).

Like Ec-NhaA, the four known crystal structures of Na^+/H^+ antiporters with the NhaA fold are dimers in which the monomers each have a conserved core domain of six helices and a less conserved dimer interface comprising additional helices. However, these dimer interfaces, unlike the dimer interface of Ec-NhaA, are composed of intertwining helices (16, 17, 19, 27). In contrast to the dimeric antiporters, the prokaryotic ASBT secondary symporters that also share the NhaA fold (20, 21) have 10 helices each and are monomeric.

To determine whether the transporters in this class have a general structure comprising a core set of helices involved primarily in transport and another set that serve mainly for assembly and/or stability of a tertiary structure, it will be necessary to determine additional crystal structures of secondary transporters that share the NhaA fold. In this regard, it is notable that variation in the number of TMs is observed within other groups of secondary transporters characterized by a common structural fold. For example, most major facilitator superfamily (MFS) members consist of 12 helices, but a few MFS members have 13, 14, or even 24 TM helices (Transporter Classification Database: www.tcdb.org and refs. 15, 34, and 35). It would be interesting to delete the "extra" helices in members of this family and examine the effect on transport activity and stability.

Materials and Methods

Plasmids, Bacterial Strains, and Culture Conditions. Plasmid pAXH3 is a pET20b (Novagen) derivative. It encodes a His-tagged NhaA (36), lacks the BglII site at position 3382, and contains a BstXI silent site at position 248 in *nha*A. A plasmid carrying a mutation is denoted according to the name of the plasmid followed by a notation of the mutational change. pAXH3-Δ(P45-N58) was previously constructed (25) and is denoted here Δβ.

EP432 is an *E. coli* K-12 derivative, which is *mel*BLid, Δ*nha*A1::*kan*, Δ*nha*B1::*cat*, Δ*lacZY*, *thr*1 (28). TA16 is *nha*A^+*nha*B^+*lacI*^{Q} and otherwise isogenic to EP432 (12). Cells were grown in either L broth (LB) or modified L broth (LBK, with NaCl replaced by KCl) (37). The medium was buffered with 60 mM 1,3 bis-{Tris (hydroxymethyl)-methylamino} propane (BTP). For plates, 1.5% agar was used. For induction, the cells were also grown in minimal medium A (38) without sodium citrate and with 0.5% (wt/vol) glycerol, 0.01% (wt/vol) $MgSO_4{\cdot}7H_2O$, and 2.5 μg/mL thiamine and threonine when needed. Antibiotics were 100 μg/mL ampicillin and/or 50 μg/mL kanamycin.

To test the mutants' resistance to Li^+ and Na^+, EP432 cells transformed with the respective plasmids were grown on LBK to OD_{600} of 0.6–0.7. Samples (4 μL) of serial 10-fold dilutions of the cultures were spotted onto selective media: LB agar plates containing the indicated concentrations of NaCl or LiCl at the various pH levels and incubated for 24 h or 48 h at 37 °C.

Mutagenesis. We used a PCR-based protocol with pAXH3 as a template. The *nha*A gene DNA of each mutation was sequenced to verify the mutation.

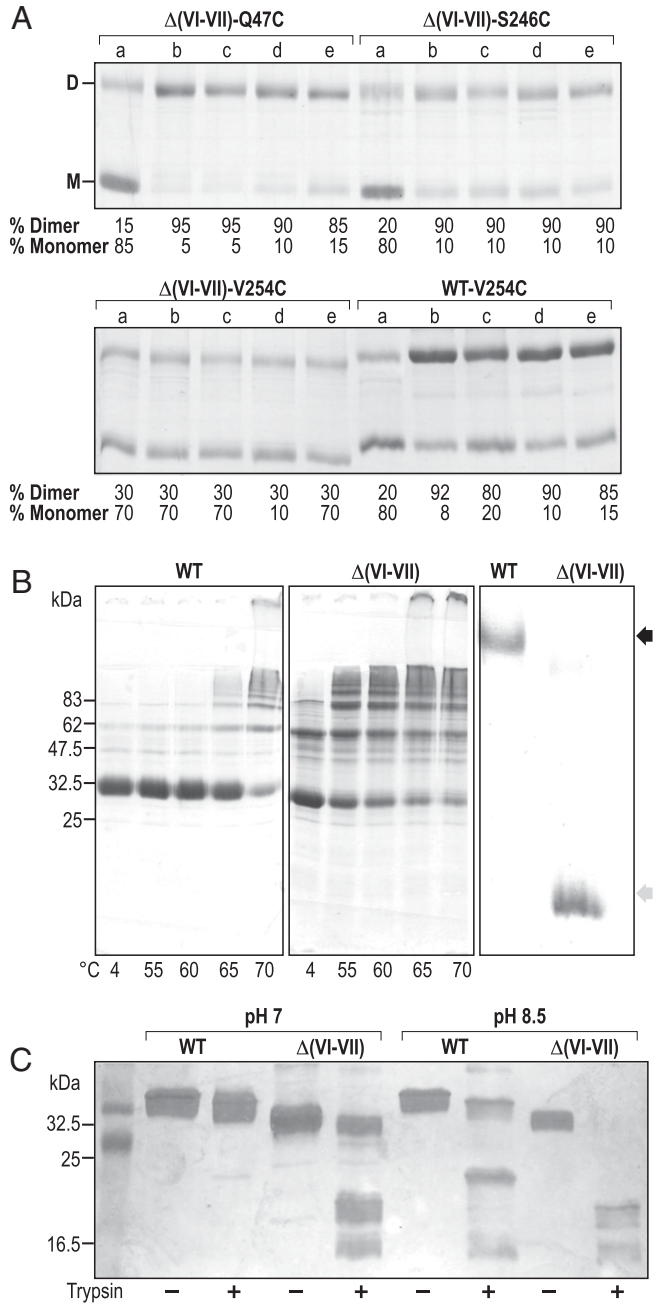

Fig. 4. The mutant Δ(VI-VII) protein in the membrane and in DDM micelles. (*A*) High-pressure membrane vesicles, expressing the indicated mutations, were treated with the cross-linkers *BMH* (lanes b), *o*-PDM (lanes c), *p*-PDM (lanes d), or MTS-2-MTS (lanes e) and nontreated control (lanes a), as described in *Materials and Methods*. The treated proteins were purified, resolved on SDS/PAGE, and Coomassie Blue-stained. When intermolecular cross-linking takes place, a band, corresponding in mobility to that of the Ec-NhaA dimer (D), appears in the gel in addition to or instead of the band representing the monomer (M). (*B*) Affinity-purified WT and mutant proteins (4 μg each) in DDM (0.03%) were incubated at the indicated temperature for 10 min, separated on SDS/PAGE, and Coomassie Blue-stained (*Left* and *Middle*). (*Right*) The WT dimer (black arrow) and the mutant monomer (gray arrow) in native gels. The position of the dimer band was previously determined by cross-linking the monomers of the dimer (25). (*C*) Affinity-purified WT and Δ(TM VI-VII) proteins in DDM micelles were subjected to trypsin digestion at the indicated pH levels for 1 h at 37 °C, and 5 μg protein samples were run on SDS/PAGE. First lane, molecular size markers. WT digestion yields heavy and light fragments only at alkaline pH, whereas digestion of the mutant is pH-independent.

Isolation of Everted Membrane Vesicles and High-Pressure Membranes and Measurement of Na^+/H^+ Antiporter Activity. Everted membrane vesicles from EP432 transformed with the respective plasmids were prepared as previously described (39, 40). High-pressure membranes were similarly prepared but the pressure for cell breakage was 20,000 psi. Everted membrane vesicles were used to determine Na^+/H^+ or Li^+/H^+ antiporter activity with an assay based on the measurement of Na^+- or Li^+-induced changes in the ΔpH as measured by acridine orange, a fluorescent probe of ΔpH. The fluorescence assay was performed in a 2.5-mL reaction mixture containing 100–150 μg membrane protein, 0.1 μM acridine orange, 150 mM choline chloride, 50 mM BTP, and 5 mM $MgCl_2$, and pH was titrated with HCl. Dequenching of fluorescence level upon addition of either Na^+ or Li^+ indicates that protons are exiting the vesicles in antiport with either cation. As shown previously, the end level of dequenching is a good estimate of antiporter activity, and the ion concentration that gives half-maximal dequenching is a good estimate of the apparent K_m of the antiporter activity (41, 42). For determination of the apparent K_m the end level of dequenching for different concentrations of the tested cations (0.01–100 mM) at the indicated pH levels was used, and the apparent K_m values were calculated by linear regression of a Lineweaver–Burk plot.

Overexpression and Purification of the NhaA Protein Variants. Overexpression of the NhaA variants and affinity purification [Ni^{+2}-nitrilotriacetic acid-agarose (Ni^{+2}-NTA; Qiagen)] were performed as described previously (31), but the protein was eluted in a buffer containing 300 mM imidazole, 25 mM citric acid, 100 mM choline chloride, 5 mM $MgCl_2$, 10% (vol/vol) glycerol, and 0.015% DDM (final pH was 7.9). Sucrose (10%) was added to the eluted protein solution, and the mixture was dialyzed overnight at 4 °C in the acidic elution buffer containing 10% (wt/vol) sucrose. The affinity-purified protein was frozen in liquid nitrogen and stored at −80 °C.

Reconstitution of NhaA Variants into Proteoliposomes and Measurement of ΔpH-Driven ^{22}Na Uptake. NhaA proteoliposomes were reconstituted, and ΔpH-driven ^{22}Na uptake was determined as described previously (12, 29). All experiments were repeated at least twice with practically identical results.

Detection and Quantitation of NhaA and Its Mutated Derivatives in the Membrane. Total membrane protein was determined according to ref. 43. The expression level of His-tagged NhaA mutants was determined by resolving the Ni-NTA–purified proteins with SDS/PAGE, staining the gels with Coomassie Blue, and using Image Gauge (Fuji software) to quantify the band densities (44).

In Situ Site-Directed Intermolecular Cross-Linking. Site-directed intermolecular cross-linking was conducted in situ on high-pressure membrane vesicles isolated from TA16 cells overexpressing the various NhaA mutants (31). Membranes (300 μg of membrane protein) were resuspended in a buffer (0.5 mL) containing 100 mM potassium phosphate (pH 7.5), 5 mM $MgSO_4$, and one of the freshly prepared homobifunctional cross-linkers: 2 mM 1,6-bismaleimidohexane (BMH; Pierce), 1mM *N*,*N*-*o*-phenylenedimaleimide (*o*-PDM; Sigma), or 2 mM MTS-2-MTS (Toronto Research Chemicals). The stock solutions of the cross-linkers were prepared in *N*,*N*-dimethylformamide so that the amount of *N*,*N*-dimethylformamide in the reaction mixture did not exceed 1%, a concentration that does not affect antiport activity. The reaction mixture was incubated at room temperature with gentle rotation for 1 h, and the reaction was terminated by 10 mM mercaptoethanol in the case of the maleimides (BMH and *o*-PDM) or by dilution in a TSC buffer [10 mM Tris·HCl (pH 7.5), 250 mM sucrose, and 140 mM choline chloride] in the case of MTS-2-MTS and centrifugation (Beckman, TLA 100.4, 26,5000 × *g*, 20 min, 4 °C). The supernatant was added to 50 μL of Ni^{+2}-NTA-agarose and incubated with agitation for 1 h at 4 °C. The beads were then washed twice in binding buffer at pH 7.4 and resuspended in 100 μL of binding buffer containing 0.2 mM fluorescein 5-maleimide (Molecular Probes) with gentle tilting for 30 min at 25 °C to determine whether Cys was accessible to the cross-linker as described (31). Then the beads were washed in washing buffer (36) at pH 7.4, and the protein was eluted in 20 μL of SDS/PAGE sampling buffer supplemented with 300 mM imidazole, agitated for 20 min at 4 °C, and collected in the supernatant after centrifugation (Eppendorf, 10,000 × *g*, 2 min, 4 °C). The affinity-purified proteins were separated on SDS/PAGE (nonreducing conditions in the case of treatment with MTS-2-MTS) and Coomassie Blue-stained to determine the densities of the bands with mobility corresponding to that of NhaA monomers and dimers. The sum of the densities of the monomers and dimers was 100%.

Blue Native-PAGE. Blue native-PAGE was carried out as previously described with small modifications for NhaA (25). The main gel and the overlay were made of 10% or 4% (wt/vol) polyacrylamide, respectively, in 0.015% DDM. The sample buffer contained 50 mM NaCl, 1 mM EDTA, 50 mM imidazole/HCl (pH 7), 0.015% DDM, and 10% glycerol. The cathode buffer contained Coomassie Blue 0.02% (G 250; Merck), and 0.015% DDM was added to both the anode and cathode buffers. The electrophoresis was conducted at 15 mA for 1 h. The gel was stained by Coomassie Blue or silver-stained and dried, and the band densities were determined as above.

Digestion by Trypsin. Affinity-purified proteins in DDM micelles were subjected to trypsin (32) in a 30-mL reaction mixture containing 10 mg of antiporter protein, 30 ng of trypsin (type III from bovine pancreas, T-8253; Sigma), 0.1% DM, 8.3 mM potassium acetate, 200 mM KCl, 6.5% glycerol, 0.7 mM Na/EDTA, 20 mM Hepes/Tris, and 1 mM $CaCl_2$. Incubation was for 60 min at 37 °C. The reaction was terminated by the addition of 100 ng of trypsin inhibitor (type II-S from soybean, T-9128; Sigma). Samples of 5 mg of protein were run on SDS/PAGE.

Determination of the Temperature Sensitivity of the Protein. Ni^2-NTA affinity-purified proteins of NhaA variants (4 μg each) were incubated at the indicated temperatures for the indicated times and separated on SDS/PAGE. The gels were Coomassie Blue-stained.

Evolutionary Conservation. The evolutionary conservation profile of NhaA was estimated using ConSurf (consurf.tau.ac.il) (22). Starting from the NhaA structure (PDB ID code 1zcd) as input, we conducted a CSI-BLAST (45) search for homologs in the Clean Uniprot database (46) with an E-value cutoff of 0.0001, minimal % ID of 15%, and maximal % ID of 99%. Of the 372 sequence hits found, 64 were unique. These were multiply aligned using MUSCLE (47), and the multiple sequence alignment was used in ConSurf calculations using the Bayesian-based estimate of the evolutionary conservation of the amino acids (48). Additional results obtained using a new (slightly refined) structure (ref. 27, PDB ID code 4au5) were, in essence, the same.

NMA. The analysis was conducted using the Gaussian network model (49) and the known structure of the transporter, as described in *SI Text*, *NMA*.

ACKNOWLEDGMENTS. T.H. acknowledges Fidan Sumbul for her help in Figs. S3–S5. This research was supported by Israel Science Foundation Grants 284/12 (to E.P.) and 1331/11 to (N.B-T.) and German Research Foundation German–Israeli Project Cooperation Grant LA3655/1-1 (to E.P. and N.B-T.).

1. Krulwich TA, Sachs G, Padan E (2011) Molecular aspects of bacterial pH sensing and homeostasis. *Nat Rev Microbiol* 9(5):330–343.
2. Padan E (2014) Functional and structural dynamics of NhaA, a prototype for Na(+) and H(+) antiporters, which are responsible for Na(+) and H(+) homeostasis in cells. *Biochim Biophys Acta* 1837(7):1047–1062.
3. Orlowski J, Grinstein S (2007) Emerging roles of alkali cation/proton exchangers in organellar homeostasis. *Curr Opin Cell Biol* 19(4):483–492.
4. Orlowski J, Grinstein S (2004) Diversity of the mammalian sodium/proton exchanger SLC9 gene family. *Pflugers Arch* 447(5):549–565.
5. Putney LK, Denker SP, Barber DL (2002) The changing face of the Na+/H+ exchanger, NHE1: Structure, regulation, and cellular actions. *Annu Rev Pharmacol Toxicol* 42:527–552.
6. Wakabayashi S, Hisamitsu T, Pang T, Shigekawa M (2003) Kinetic dissection of two distinct proton binding sites in Na^+/H^+ exchangers by measurement of reverse mode reaction. *J Biol Chem* 278(44):43580–43585.
7. Fliegel L (2008) Molecular biology of the myocardial Na+/H+ exchanger. *J Mol Cell Cardiol* 44(2):228–237.
8. Padan E, Bibi E, Ito M, Krulwich TA (2005) Alkaline pH homeostasis in bacteria: New insights. *Biochim Biophys Acta* 1717(2):67–88.
9. Lescat M, et al. (2014) The conserved nhaAR operon is drastically divergent between B2 and non-B2 Escherichia coli and is involved in extra-intestinal virulence. *PLoS One* 9(9):e108738.
10. Kondapalli KC, Kallay LM, Muszelik M, Rao R (2012) Unconventional chemiosmotic coupling of NHA2, a mammalian Na+/H+ antiporter, to a plasma membrane H+ gradient. *J Biol Chem* 287(43):36239–36250.
11. Deisl C, et al. (2013) Sodium/hydrogen exchanger NHA2 is critical for insulin secretion in β-cells. *Proc Natl Acad Sci USA* 110(24):10004–10009.
12. Taglicht D, Padan E, Schuldiner S (1991) Overproduction and purification of a functional Na^+/H^+ antiporter coded by *nhaA* (*ant*) from *Escherichia coli*. *J Biol Chem* 266(17):11289–11294.
13. Taglicht D, Padan E, Schuldiner S (1993) Proton-sodium stoichiometry of NhaA, an electrogenic antiporter from *Escherichia coli*. *J Biol Chem* 268(8):5382–5387.
14. Hunte C, et al. (2005) Structure of a Na^+/H^+ antiporter and insights into mechanism of action and regulation by pH. *Nature* 435(7046):1197–1202.
15. Shi Y (2013) Common folds and transport mechanisms of secondary active transporters. *Annu Rev Biophys* 42:51–72.
16. Wöhlert D, Kühlbrandt W, Yildiz O (2014) Structure and substrate ion binding in the sodium/proton antiporter PaNhaP. *eLife* 3:e03579.
17. Paulino C, Wöhlert D, Kapotova E, Yildiz Ö, Kühlbrandt W (2014) Structure and transport mechanism of the sodium/proton antiporter MjNhaP1. *eLife* 3:e03583.
18. Schushan M, et al. (2012) A model-structure of a periplasm-facing state of the NhaA antiporter suggests the molecular underpinnings of pH-induced conformational changes. *J Biol Chem* 287(22):18249–18261.
19. Lee C, et al. (2013) A two-domain elevator mechanism for sodium/proton antiport. *Nature* 501(7468):573–577.
20. Hu NJ, Iwata S, Cameron AD, Drew D (2011) Crystal structure of a bacterial homologue of the bile acid sodium symporter ASBT. *Nature* 478(7369):408–411.
21. Zhou X, et al. (2014) Structural basis of the alternating-access mechanism in a bile acid transporter. *Nature* 505(7484):569–573.
22. Celniker G, et al. (2013) ConSurf: Using evolutionary data to rase testable hupothesis about protein function. *Is J Chem* 53(3–4):199–206.
23. Haliloglu T, Bahar I, Erman B (1997) Gaussian dynamics of folded proteins. *Phys Rev Lett* 79:3090–3093.
24. Padan E, Kozachkov L, Herz K, Rimon A (2009) NhaA crystal structure: Functional-structural insights. *J Exp Biol* 212(Pt 11):1593–1603.
25. Rimon A, Tzubery T, Padan E (2007) Monomers of the NhaA Na+/H+ antiporter of Escherichia coli are fully functional yet dimers are beneficial under extreme stress conditions at alkaline pH in the presence of Na+ or Li+. *J Biol Chem* 282(37):26810–26821.
26. Herz K, Rimon A, Jeschke G, Padan E (2009) Beta-sheet-dependent dimerization is essential for the stability of NhaA Na+/H+ antiporter. *J Biol Chem* 284(10):6337–6347.
27. Lee C, et al. (2014) Crystal structure of the sodium-proton antiporter NhaA dimer and new mechanistic insights. *J Gen Physiol* 144(6):529–544.
28. Pinner E, Kotler Y, Padan E, Schuldiner S (1993) Physiological role of *nhaB*, a specific Na^+/H^+ antiporter in *Escherichia coli*. *J Biol Chem* 268(3):1729–1734.
29. Rimon A, Gerchman Y, Kariv Z, Padan E (1998) A point mutation (G338S) and its suppressor mutations affect both the pH response of the NhaA-Na^+/H^+ antiporter as well as the growth phenotype of *Escherichia coli*. *J Biol Chem* 273(41):26470–26476.
30. Williams KA, Geldmacher-Kaufer U, Padan E, Schuldiner S, Kühlbrandt W (1999) Projection structure of NhaA, a secondary transporter from Escherichia coli, at 4.0 A resolution. *EMBO J* 18(13):3558–3563.
31. Tzubery T, Rimon A, Padan E (2008) Structure-based functional study reveals multiple roles of transmembrane segment IX and loop VIII-IX in NhaA Na+/H+ antiporter of Escherichia coli at physiological pH. *J Biol Chem* 283(23):15975–15987.
32. Gerchman Y, Rimon A, Padan E (1999) A pH-dependent conformational change of NhaA $Na^{(+)}/H^{(+)}$ antiporter of *Escherichia coli* involves loop VIII-IX, plays a role in the pH response of the protein, and is maintained by the pure protein in dodecyl maltoside. *J Biol Chem* 274(35):24617–24624.
33. Kozachkov L, Padan E (2013) Conformational changes in NhaA Na^+/H^+ antiporter. *Mol Membr Biol* 30(1):90–100.
34. Zhao Y, et al. (2014) Crystal structure of the E. coli peptide transporter YbgH. *Structure* 22(8):1152–1160.
35. Reddy VS, Shlykov MA, Castillo R, Sun EI, Saier MH, Jr (2012) The major facilitator superfamily (MFS) revisited. *FEBS J* 279(11):2022–2035.
36. Olami Y, Rimon A, Gerchman Y, Rothman A, Padan E (1997) Histidine 225, a residue of the NhaA-Na^+/H^+ antiporter of *Escherichia coli* is exposed and faces the cell exterior. *J Biol Chem* 272(3):1761–1768.
37. Padan E, Maisler N, Taglicht D, Karpel R, Schuldiner S (1989) Deletion of *ant* in *Escherichia coli* reveals its function in adaptation to high salinity and an alternative Na^+/H^+ antiporter system(s). *J Biol Chem* 264(34):20297–20302.
38. Davis BD, Mingioli ES (1950) Mutants of Escherichia coli requiring methionine or vitamin B12. *J Bacteriol* 60(1):17–28.
39. Rosen BP (1986) Ion extrusion systems in Escherichia coli. *Methods Enzymol* 125:328–336.
40. Goldberg EB, et al. (1987) Characterization of a Na^+/H^+ antiporter gene of *Escherichia coli*. *Proc Natl Acad Sci USA* 84(9):2615–2619.
41. Schuldiner S, Fishkes H (1978) Sodium-proton antiport in isolated membrane vesicles of Escherichia coli. *Biochemistry* 17(4):706–711.
42. Tsuboi Y, Inoue H, Nakamura N, Kanazawa H (2003) Identification of membrane domains of the Na^+/H^+ antiporter (NhaA) protein from Helicobacter pylori required for ion transport and pH sensing. *J Biol Chem* 278(24):21467–21473.
43. Bradford MM (1976) A rapid and sensitive method for the quantitation of microgram quantities of protein utilizing the principle of protein-dye binding. *Anal Biochem* 72:248–254.
44. Gerchman Y, Rimon A, Venturi M, Padan E (2001) Oligomerization of NhaA, the Na^+/H^+ antiporter of *Escherichia coli* in the membrane and its functional and structural consequences. *Biochemistry* 40(11):3403–3412.
45. Biegert A, Söding J (2009) Sequence context-specific profiles for homology searching. *Proc Natl Acad Sci USA* 106(10):3770–3775.
46. Consortium TU; UniProt Consortium (2008) The universal protein resource (UniProt). *Nucleic Acids Res* 36(Database issue):D190–D195.
47. Edgar RC (2004) MUSCLE: multiple sequence alignment with high accuracy and high throughput. *Nucleic Acids Res* 32:1792–1797.
48. Mayrose I, Graur D, Ben-Tal N, Pupko T (2004) Comparison of site-specific rate-inference methods for protein sequences: Empirical Bayesian methods are superior. *Mol Biol Evol* 21(9):1781–1791.
49. Bahar I, Atilgan AR, Erman B (1997) Direct evaluation of thermal fluctuations in protein using a single parameter harmonic potential. *Folding Des* 2:173–181.